(2)

Naval Research Laboratory
Washington, DC 20375-5000

NRL Memorandum Report 6609

Diffraction Effects in Directed Radiation Beams

B. HAFIZI* AND P. SPRANGLE

Beam Physics Branch
Plasma Physics Division

**Science Applications Intl. Corp., McLean, VA 22102*

April 3, 1990

REPORT DOCUMENTATION PAGE

Form Approved
OMB No 0704-0188

1. AGENCY USE ONLY *(Leave blank)*

2. REPORT DATE: 1990 April 3

3. REPORT TYPE AND DATES COVERED: Interim

4. TITLE AND SUBTITLE: Diffraction Effects in Directed Radiation Beams

5. FUNDING NUMBERS: 47-2005-0-0 (JO#)
DOE Contract #
AI05-83ER40117

6. AUTHOR(S): B. Hafizi* and P. Sprangle

7. PERFORMING ORGANIZATION NAME(S) AND ADDRESS(ES):
Naval Research Laboratory
Code 4790
Washington, DC 20375-5000

8. PERFORMING ORGANIZATION REPORT NUMBER: NRL Memorandum Report 6609

9. SPONSORING/MONITORING AGENCY NAME(S) AND ADDRESS(ES):
DOE
Washington, DC 20545

10. SPONSORING/MONITORING AGENCY REPORT NUMBER

11. SUPPLEMENTARY NOTES:
*Science Applications Intl. Corp., McLean, VA 22102

12a. DISTRIBUTION/AVAILABILITY STATEMENT:
Approved for public release;
unlimited.

12b. DISTRIBUTION CODE

13. ABSTRACT *(Maximum 200 words)*
A number of proposed applications of electromagnetic waves require that the radiation beam maintain a high intensity over an appreciable propagation distance. These applications include, among others, power beaming, advanced radar, laser acceleration of particles and directed-energy sources. The quest to achieve these objectives has led to a resurgence of research on diffraction theory. This report presents a survey and critique of the analyses and experimental tests of solutions of the wave equation in connection with so-called diffractionless and other directed radiation beams. The examples discussed in this paper include electromagnetic missiles, Bessel beams, electromagnetic directed energy pulse trains, and electromagnetic bullets.

14. SUBJECT TERMS:
Directed radiation beams
Electromagnetic missiles
Bessel beams
Electromagnetic directed energy pulse trains
Electromagnetic bullets
Diffraction effects

15. NUMBER OF PAGES: 60

16. PRICE CODE

17. SECURITY CLASSIFICATION OF REPORT	18. SECURITY CLASSIFICATION OF THIS PAGE	19. SECURITY CLASSIFICATION OF ABSTRACT	20. LIMITATION OF ABSTRACT
UNCLASSIFIED	UNCLASSIFIED	UNCLASSIFIED	SAR

NSN 7540-01-280-5500

Standard Form 298 (Rev. 2-89)

Contents

DIFFRACTION EFFECTS IN DIRECTED RADIATION BEAMS

I. Introduction and Summary

Diffraction is a fundamental characteristic of all wave fields, be it photons, electrons, etc. The effect of diffraction is typically manifested when an obstacle is placed in the path of a beam. On an observation screen some distance away from the obstacle one observes a rather complicated modulation of the time-average intensity in the vicinity of the boundary separating the illuminated region from the geometrical shadow cast by the obstacle.

In many applications it would be highly desirable to propagate a beam over a long distance without an appreciable drop in the intensity. As an example we cite the possibility of accelerating particles to ultra-high energies by utilizing high-power laser beams. Although the accelerating gradient in many of these schemes is extremely large, the actual distance over which the particle and laser beams maintain an appreciable overlap is very limited. The overlap is reduced due to the diffraction of the laser beam and as a result the net gain in the particle energy is limited.

With the advent of high-power lasers and microwave sources, diffraction of radiation beams with finite transverse dimensions has turned into a problem of special importance. As an example, consider laser radiation of frequency ω emanating from a cavity oscillating in the fundamental transverse Gaussian mode. How far will this beam propagate in a turbulence-free atmosphere? More to the point, how fast is the fall-off in the intensity of this laser beam?

The answer to this question is well-known.[1] The scale length for the fall-off in intensity is given by the Rayleigh range, defined by

$$Z_R \equiv \pi w_0^2/\lambda, \tag{1}$$

Manuscript approved February 16, 1990

where w_o is the minimum spot size, or radius, of the beam, and $\lambda = 2\pi c/\omega$ is the wavelength. The minimum spot size w_o is also known as the waist of the radiation beam. The fall-off of the beam intensity as it propagates in space is a consequence of the fact that initially the beam was constrained to a finite waist, w_o. Diffraction then causes the beam to spread in the lateral direction and, from energy conservation, the intensity must drop off correspondingly. In the limit of an infinitely wide beam, $w_o \to \infty$, the Rayleigh range is infinite, there is no diffraction and the intensity is constant.

A natural way to propagate a beam over long distances is to increase the Rayleigh range by employing a wider beam or shorter wavelength radiation. Clearly the width of the beam is limited by the energy source available for pumping the lasing medium, and short wavelength lasers (x-rays and beyond) are not presently available. As a result, over the past several years there has been an upsurge in research on such fundamental topics as propagation and diffraction properties of radiation beams. (See Ref. 2 for an earlier discussion.) Briefly, the question being asked is: "Can diffraction be overcome?" The following is a summary of our review of diffractionless and other directed radiation beams.

i) Electromagnetic Missiles (Section IV)

Experiments indicate the possibility of generating wave packets with a broad frequency spectrum. The high-frequency end of the spectrum determines the furthest distance the missile can propagate, in complete accord with our understanding of diffraction.

ii) Bessel Beams (Section V)

A Bessel beam is a particular, monochromatic solution of the wave equation. Bessel beams propagate no further than Gaussian beams or plane waves with the same transverse dimensions and, contrary to previous assertions, Bessel beams are not "resistant to the diffractive spreading commonly associated with all wave propagation".

iii) Electromagnetic Directed Energy Pulse Trains (Section VI)

These are particular, broad-band solutions of the wave equation. We show that the experiment and the numerical studies of these pulses are consistent with conventional diffraction theory and, contrary to previous assertions, these pulses do not "defeat diffraction".

iv) Electromagnetic Bullets (Section VII)

Electromagnetic bullets are solutions of the wave equation which are confined to a finite region of space in the wave-zone. The ultimate goal of the research has been to determine the source function which leads to a prescribed form for the bullet in the wave-zone. Although the mathematical framework for this has been established, no concrete example has appeared in the literature.

Sections II and III begin with a review of basic diffraction theory and our findings and conclusions are summarized in Section VIII.

II. Electromagnetic Wave Diffraction

Consider the radiation beam from a cavity of radius d. The wave vector is given by $k_{\parallel}\hat{e}_z$, corresponding to propagation predominantly in the z direction, and the magnitude of the spread in the wave vector in the transverse direction is denoted by $\Delta k_{\perp}$, with $k_{\parallel} >> \Delta k_{\perp}$. The angular spread of the radiation relative to the z axis is

$$\theta \simeq \Delta k_{\perp}/k_{\parallel}. \qquad (2)$$

On an observation screen at a distance z, the radius of the illuminated region is given by

$$w \simeq d + \theta z. \qquad (3)$$

The first term on the right-hand side of this expression indicates the width of the region illuminated according to geometrical optics. Beyond this lies the region of the geometrical shadow, and the second term in Eq. (3) indicates the extent to which this region is illuminated due to diffraction of light. The distance Z over which the angular spread leads to a fall-off in the intensity is given by $d + \theta Z = 2d$, or

$$Z = d/\theta. \qquad (4a)$$

The distance Z may be regarded as the scale-length for diffractive spreading of the beam.

As a first example, suppose the transverse distribution of intensity in the beam is uniform. This is the case when plane waves are apertured. If the radius of the aperture is d, from a fundamental result of Fourier analysis, $\Delta k_{\perp} d \simeq 1$. The angular spread is therefore given by $\theta \simeq \lambda/2\pi d$, where $\lambda = 2\pi/k_{\parallel}$ is the wavelength. For this intensity distribution one thus finds

$$Z_p \approx 2\pi d^2/\lambda. \tag{4b}$$

For the case when the transverse intensity distribution is a Gaussian, $\exp(-r^2/w_o^2)$, of width w_o, we have $\Delta k_\perp \approx 1/w_o$, and the angular spread of the beam is on the order of $\theta \approx \lambda/2\pi w_o$. In this case $d = w_o$ and hence

$$Z_G \approx 2\pi w_o^2/\lambda, \tag{4c}$$

which is twice the Rayleigh range Z_R defined in Eq. (1).

Clearly, diffraction is simply the physical manifestation of the well-known result of Fourier analysis relating the spreads in wave vector space with the corresponding widths in real space, $\Delta k_i \Delta x_i \approx 1$ for $i = 1,2,3$. As a result, Eq. (4a) expresses a fundamental relation which we shall make use of repeatedly in order to interpret the results of theory and experiment on so-called diffractionless radiation beams.

III. Diffraction Zones (Huygens' Principle)

According to Huygens' principle each point on a given wavefront acts as a source of secondary wavelets. The field at a point P is given by the sum over the wavelets. If $u(\underline{r})e^{-i\omega t}$ is the amplitude on an aperture, an approximate solution of the scalar wave equation at P is given by[3,4]

$$\psi_p(\underline{r},t) = (i\lambda)^{-1} e^{-i\omega t} \int_{\text{aperture}} dS' \; u(\underline{r}') \, R^{-1} \, e^{i\omega R/c}, \tag{5}$$

where $R = [(x-x')^2 + (y-y')^2 + z^2]^{1/2}$ is the distance between the area element dS' on the aperture and the point P, as shown in Fig. 1.

In the Fresnel approximation the binomial expansion of R may be used to simplify Eq. (5) to

$$\psi_p \propto (i\lambda z)^{-1} e^{i\omega(z-ct)/c} \int_{\text{aperture}} dS' \; u(x',y') \; e^{i\frac{\omega}{c}\left(\frac{x'^2 + y'^2}{2z} - \frac{xx' + yy'}{z}\right)}. \tag{6}$$

For plane waves incident on an aperture with linear dimension d, there are two physically interesting limits for approximating Eq. (6).

i) Fraunhofer Diffraction (Far-Field or Wave-Zone Region)

If

$$z \gg d^2/\lambda, \tag{7}$$

one may neglect the quadratic terms in the exponent of Eq. (6) and the wavelets from the entire wavefront at the aperture contribute to the field at P. In the Fraunhofer region ψ_p is simply the Fourier transform of the amplitude at the diffracting aperture.

ii) Fresnel Diffraction (Near-Field Region)

In the other limit,

$$z < d^2/\lambda, \tag{8}$$

it is necessary to retain the quadratic terms in the exponent of Eq. (6) and the wavelets from a limited portion of the wavefront at the aperture make the dominant contribution to the field at P. In this case, the integration in Eq. (6) may be taken to be over the entire $z = 0$ plane.

For plane waves incident on a circular aperture of radius d, Fig. 2, making use of Eq. (5), the exact field on the axis of symmetry is given by $\psi_P \propto \exp(-i\omega t)\{\exp(i\omega z/c) - \exp[i\omega(d^2 + z^2)^{1/2}/c]\}$, and the intensity $I \propto \psi_P \psi_P^*$ is

$$I \propto 1 - \cos \{\omega[(d^2 + z^2)^{1/2} - z]/c\}. \qquad (9)$$

Figure 3 is a schematic plot of the intensity function, Eq. (9), indicating in particular the transition between the Fresnel and the Fraunhofer regions. Note that the intensity drops off precipitously beyond $z \simeq 2\pi d^2/\lambda$, consistent with the scale-length defined by Eq. (4b).

We proceed now to examine the research on new solutions of the wave equation, with particular emphasis on their diffraction properties.[5-20]

IV. Electromagnetic Missiles

i) Theory

Consider first the case of a field, termed a "missile", which falls off more slowly than the usual $1/R$ law. The inventive step is the use of a broad frequency spectrum. Depending on the spectrum, the fall-off with R may be as slow as desired.[7,8]

To appreciate the nature of this field, note that for an arbitrary source distribution within a region A as shown in Fig. 4, the energy delivered to a screen S, integrated over all time, is

$$\varepsilon(S,R) = \int_{-\infty}^{\infty} dt \int_{\text{screen}} dS\, \hat{n} \cdot (\underline{E} \times \underline{B})/4\pi,$$

where $\hat{n}$ is a unit vector normal to the screen, and $\underline{E}$ and $\underline{B}$ are the electric and the magnetic field, respectively. For a source with a bounded frequency spectrum, a screen of fixed area S, and for sufficiently large R, $\varepsilon(S,R) \sim 1/R^2$, according to well-known results.[21]

The current density for the electromagnetic missile described in Ref. 7, $\underline{J}(\underline{r},t) = \delta(z)f(t)\hat{e}_x$, $r < d$, is confined to a disk of radius d, where $r = (x^2 + y^2)^{1/2}$ is the radial coordinate and $f(t)$ is a given function of time. If $\tilde{\underline{A}}(\omega)$ and $\tilde{\underline{J}}(\omega)$ denote the Fourier transforms of the vector potential and the current density respectively, then $\tilde{\underline{A}}(\omega) = \int d^3r\, \tilde{\underline{J}}(\omega)\exp(i\omega R/c)/cR$ is a solution of the wave equation.[21] In the present case, $\tilde{\underline{J}}(\omega) = \delta(z)\tilde{f}(\omega)\hat{e}_x$, and the vector potential on the axis of symmetry is given by

$$\tilde{\underline{A}}(\omega) = \frac{2\pi}{c}\, \tilde{f}(\omega) \int_0^d dr\, r\, (r^2 + z^2)^{-1/2}\, e^{i\frac{\omega}{c}(r^2 + z^2)^{1/2}}\, \hat{e}_x.$$

Making use of this expression for $\tilde{\underline{A}}(\omega)$, the Poynting flux along the z axis integrated over all time, $U(z) \equiv \int dt\, \hat{e}_z \cdot (\underline{E} \times \underline{B})/4\pi$, is given by

$$U = c^{-2}[1 + z(z^2 + d^2)^{-1/2}] \int_0^\infty d\omega \left|\tilde{f}(\omega)\right|^2 \left(1 - \cos\{\tfrac{\omega}{c}[(z^2 + d^2)^{1/2} - z]\}\right). \tag{10}$$

Note the resemblance between Eq. (9) and the integrand of Eq. (10). Equation (9) is for a monochromatic field and is based on Huygens-Fresnel principle while Eq. (10) is obtained from a rigorous solution of the full wave equation.

In the limit $z \to \infty$ in Eq. (10), for a fixed frequency ω, $\cos\{(\omega/c)[(z^2+d^2)^{1/2} - z]\} \to \cos(\omega d^2/2cz) \to 1$, and the integrand tends to zero. Referring to Fig. 3, this means that the contribution of this frequency lies in the far-field region and is thus negligible. At a given large z we can, therefore, write

$$U \simeq \frac{2}{c^2} \int_{2cz/d^2}^{\infty} d\omega \left|\tilde{f}(\omega)\right|^2 [1 - \cos(\omega d^2/2cz)] \simeq \frac{2}{c^2} \int_{2cz/d^2}^{\infty} d\omega \left|\tilde{f}(\omega)\right|^2 .$$

We see that the most important contribution is from the high frequency end of the spectrum, for which the given point z lies in the near-field, Fresnel, zone. The contributions from all the lower frequency components will have decayed to negligible values before reaching the given z. While the eventual fall off of any frequency component is as 1/z, the fall-off of the time integrated Poynting flux for the wave packet depends on how rapidly $|\tilde{f}(\omega)|$ decays for $\omega > 2cz/d^2$. As an example, consider a source with a frequency response

$$\tilde{f}(\omega) = [1 + (\omega/\omega_0)^2]^{(1+2\epsilon)/4},$$

where $\varepsilon > 0$. For this spectrum the time-integrated Poynting flux falls off as $U \propto 1/z^{2\varepsilon}$. The fall-off can thus be as slow as desired by taking the limit $\varepsilon \to 0$. The limit, however, corresponds to a frequency spectrum from a source with infinite energy. The function f(t) is symmetric with respect to $t \to -t$. Evaluating the inverse Fourier transform of $\tilde{f}(\omega)$, one finds that $f(t) \sim t^{(2\varepsilon-3)/4}\exp(-\omega_0 t)$ for $t \gg 1/\omega_0$. For $\varepsilon > 1/2$ and $t \ll 1/\omega_0$, $f(t) \to$ constant. However, for the more interesting case of $\varepsilon < 1/2$, $f(t) \to t^{\varepsilon-1/2}$ when $t \ll 1/\omega_0$, indicating a mild singularity.

ii) Experiment (Electromagnetic Missiles)

The difficulties involved in an experimental study of electromagnetic missiles stem from the need to generate pulses with extremely short rise-times and suitably-shaped wavefronts.[9] An antenna was used to generate a "pure" spherical wave which formed the primary pulse and the field reflected from a parabolic dish of radius 2 ft formed the secondary pulse. The pulses were detected by a specially-designed sensor. The primary pulse was found to fall off as $1/z^2$, the energy decaying by 1/16 when the sensor was moved from 4 ft to 16 ft from the source. This was because the antenna, being a point source, generated spherical wavefronts. The pulse reflected from the parabolic dish was found to resemble that of a circular disk, similar to that studied earlier in this section. Over the same distance, the energy in this electromagnetic missile was found to decay by just under 1/2. Without a precise knowledge of the frequency spectrum it is not possible to make a quantitative analysis of this experiment. Rough estimates indicate that the scale length for the fall-off of the intensity of the missile is indeed compatible with the diffraction scale length $Z = 2\pi d^2/\lambda$, where d = 2 ft is the radius of the reflecting dish and λ is the wavelength for the highest frequency (10 GHz) in the pulse.

These preliminary experimental results indicate that a suitably tailored pulse-shape can be designed to have an energy-decay rate essentially limited by the highest frequencies present in the pulse generator, in complete accordance with the elementary notions of diffraction of light. Propagation of a composite pulse in free space is a dispersive process. As the beam propagates, the lowest frequency components diffract away first.

V. Bessel Beams

i) Theory

An example of a so-called diffractionless electromagnetic beam is a Bessel beam. We note that a particular solution of the scalar wave equation

$$\left(\nabla^2 - c^{-2}\frac{\partial^2}{\partial t^2}\right)\psi(\underline{r},t) = 0,$$

is

$$\psi = e^{i(k_{\parallel}z - \omega t)}\int_{\theta_o}^{2\pi+\theta_o} d\theta\, A(\theta) e^{ik_{\perp}(x\cos\theta + y\sin\theta)}, \qquad (11)$$

for arbitrary θ_o and $A(\theta)$, provided $\omega^2 = c^2(k_{\parallel}^2 + k_{\perp}^2)$. Here, $k_{\parallel}$ and $k_{\perp}$ denote the magnitudes of the components of the wave vector parallel and orthogonal to the z axis, respectively, and $\lambda = 2\pi/(k_{\parallel}^2 + k_{\perp}^2)^{1/2}$ is the wavelength. Since the z-dependence in Eq. (11) is separated from the x- and y-dependence, the solution is clearly diffractionless in the sense that the time-average intensity is independent of z. In fact, the intensity is constant for all z and all t.

Durnin considers the case where $A(\theta) = 1$ (Ref. 10). In this case, making use of the expansion $\exp(i\zeta\sin\theta) = \Sigma_n J_n(\zeta)\exp(in\theta)$, where J_n is the ordinary Bessel function of the first kind of order n (Ref. 22), Eq. (11) simplifies to $\psi = 2\pi J_o(k_{\perp}r)\exp[i(k_{\parallel}z - \omega t)]$, where $r = (x^2 + y^2)^{1/2}$ is the radial variable.

Making use of the properties of the Bessel function (Ref. 22), one can show that the "energy" content, $\int dr\, r\, J_o^2(k_{\perp}r)$, integrated over any transverse period, or lobe, is approximately the same as that in the central lobe. This point will be important in our interpretation of the diffractive properties of Bessel beams.

ii) Experiment (Bessel Beams)

A Bessel beam has an infinite number of lobes and, therefore, has infinite energy. In the laboratory an approximation to this ideal beam is realized by clipping the beam beyond a certain radius. The question is, given the finite transverse size, how well is the diffractionless property preserved.

To answer this question Durnin et al. compared the propagation of a clipped Bessel beam with a Gaussian beam.[11] The full width at half-maximum (FWHM) of the Gaussian was taken to be equal to the FWHM of the central lobe of the Bessel beam. In the experiment the on-axis intensity of each beam was measured along the axis of symmetry. The Bessel beam was claimed to be "resistant to the diffractive spreading commonly associated with all wave propagation" since its intensity was observed to remain approximately constant for a much longer distance than the Gaussian beam. The idea of a diffraction-free beam was further reinforced by using a geometrical optics argument to obtain a formula for the propagation distance of central lobe of the Bessel beam.

We shall now reconsider this comparison. The wavelength of the radiation was $\lambda = 6328$ Å. For the Gaussian beam, $\exp(-r^2/w_0^2)$, w_0 was equal to 0.042 mm, corresponding to a FWHM of 0.07 mm. For the Bessel beam, $J_0(k_\perp r)$, $k_\perp$ was equal to 41 mm^{-1}, corresponding to a FWHM for the central lobe of 0.07 mm. The beams were apertured to a radius $d = 3.5$ mm. The following order-of-magnitude discussion is based on Eqs. (2)-(4); a more rigorous analysis is presented in the Appendix. The angular spread due to the natural width of the Gaussian beam is $\theta = \lambda/2\pi w_0$ and Eq. (3) takes the form $w = w_o + (\lambda/2\pi w_o)z$, where the first term in this expression is w_o, rather than d, since the energy of the Gaussian is concentrated in the central peak. The scale length for diffraction is the same as that given by Eq. (4c), namely $Z_G \approx 2\pi w_o^2/\lambda = 1.75$ cm. The natural angular spread of the Bessel beam is $\theta = k_\perp \lambda/2\pi$, and Eq. (3) takes the form $w = d + (k_\perp \lambda/2\pi)z$, where the first term represents the radius of the aperture since the energy in each lobe is approximately the same and they all affect the propagation of the Bessel beam. The scale length for diffraction is, therefore, given by $d + (k_\perp \lambda/2\pi)Z_B = 2d$, or $Z_B \approx 2\pi d/k_\perp \lambda \approx 85$ cm, which is consistent with the experimental observation.

In the transverse plane the lobes of the Bessel beam diffract away sequentially starting with the outermost one. The outermost lobe diffracts in a distance on the order of $2\pi^2/\lambda k_\perp^2$, which is approximately equal to Z_G. The next lobe diffracts away after a distance on the order of $2Z_G$. This process continues until the central lobe, which diffracts away after a distance $\sim NZ_G$, where N denotes the number of lobes within the aperture. In the experiment $N \approx 50$, implying a propagation distance on the order of $50Z_G$ for the central lobe of the Bessel beam, which is consistent with the measured value. Measurements of the on-axis intensity obviously fail to reveal the gradual deterioration of the transverse beam profile, but the numerical plots in Fig. 2 of Ref. 10 are consistent with this scenario. Therefore, the Bessel beam is not "resistant to the diffractive spreading commonly associated with all wave propagation". Our interpretation points out the significance of each successive lobe having about the same energy. The central lobe persists as long as there are off-axis lobes compensating for its energy loss and hence the comparison with the narrower Gaussian beam in Ref. 11 is of little significance.

We note that utilizing the full width of the aperture a Gaussian beam propagates a distance on the order of NZ_B; i.e., N times further than the Bessel beam. Additionally, by appropriately curving the wavefront, nearly all the power of the Gaussian beam can be focussed on a target of dimension w_c in a distance Z_B. Hence, for this purpose a Gaussian beam would be significantly better than the Bessel beam employed by Durnin et al. (See also Ref. 12)

VI. Electromagnetic Directed Energy Pulse Trains

i) Theory

Electromagnetic directed energy pulse trains are particular solutions of Maxwell's equations.[13] To discuss these, we make the change of variables $\xi = z - ct$ and $\tau = t$, and transform the wave equation

$$\left(\nabla^2 - c^{-2}\ \partial^2/\partial t^2\right)\Psi = 0,$$

into the form

$$\left(\nabla_\perp^2 + \frac{2}{c}\frac{\partial^2}{\partial\xi\partial\tau} - c^{-2}\ \partial^2/\partial\tau^2\right)\Psi = 0.$$

Making the assumption

$$\Psi = \psi(\xi,r,\tau)e^{i\omega\xi/c}, \qquad (12)$$

leads to the an equation for the complex envelope ψ.

$$\left(\nabla_\perp^2 + 2i\omega c^{-2}\ \frac{\partial}{\partial\tau} + \frac{2}{c}\frac{\partial^2}{\partial\tau\partial\xi} - c^{-2}\ \frac{\partial^2}{\partial\tau^2}\right)\psi = 0.$$

Here, r denotes the radial variable and $\nabla_\perp$ is the differential operator in the plane z = constant. If $\psi(\xi,r,\tau)$ varies slowly compared to the characteristic scales $1/\omega$ and c/ω, the second derivative of the envelope function may be neglected and the wave equation reduces to

$$\left(\nabla_\perp^2 + 2i\omega\ c^{-2}\ \frac{\partial}{\partial\tau}\right)\psi = 0. \qquad (13)$$

Equation (13) is an extremely useful approximation to the full wave equation in a vacuum. Note that the full wave operator is of the hyperbolic type, whereas the reduced wave operator is of the parabolic type. For this reason, Eq. (13) is sometimes referred to as the parabolic approximation to the wave equation.

A particular solution of Eq. (13) is given by

$$\psi = C \frac{w_o}{w} e^{-i\tan^{-1}(\tau/\tau_R) - (1-i\tau/\tau_R)r^2/w^2}, \tag{14a}$$

where C is a constant,

$$w = w_o \left[1 + (\tau/\tau_R)^2\right]^{1/2}, \tag{14b}$$

is the spot size, w_o is the waist and

$$\tau_R = \omega w_o^2 /2c^2, \tag{14c}$$

is related to the Rayleigh range $Z_R = \omega w_o^2/2c$ by $\tau_R = Z_R/c$.

Ziolkowski[13-15] makes use of the variables transformation

$$\xi = z - ct, \qquad \eta = z + ct,$$

in the wave equation to reduce it to the form

$$\left(\nabla_\perp^2 + 4 \frac{\partial^2}{\partial\eta\partial\xi}\right)\Psi = 0.$$

Representing Ψ in the form

$$\Psi = \psi(\eta, r)e^{i\omega\xi/c}, \tag{15}$$

leads, without any approximation, to an equation for ψ,

$$\left(\nabla_\perp^2 + 4i \frac{\omega}{c} \frac{\partial}{\partial\eta}\right)\psi = 0. \tag{16}$$

A particular solution of Eq. (16) is given by

$$\psi = C \frac{w_o}{w} e^{-i\tan^{-1}(\eta/\eta_R) - (1-i\eta/\eta_R)r^2/w^2}, \tag{17a}$$

where C is a constant,

$$w = w_o \left[1 + (\eta/\eta_R)^2\right]^{1/2}, \tag{17b}$$

and

$$\eta_R = \omega w_o^2/c, \tag{17c}$$

is related to the Rayleigh range $Z_R = \omega w_o^2/2c$ by $\eta_R = 2Z_R$.

Some remarks on the solutions in Eqs. (14) and (17) are in order. First, Eq. (14) is a solution of the parabolic approximation to the full wave equation. On the other hand, Eq. (17) is an exact solution of the full equation. Second, there is a factor-of-two difference between the scale length $c\tau_R$ in Eq. (14c) and the scale length η_R in Eq. (17c). Third, the solution in Eq. (17) has infinite energy. Finally, the exact solution in Eq. (15) consists of a pulse traveling to the left which is modulated by a plane wave moving to the right.

To examine the last two points, Eqs. (15) and (17) may be combined to form a fundamental Gaussian pulse Ψ_k with parameter $k = \omega/c$

$$\Psi_k(r,z,t) = e^{ik\eta} \frac{e^{-kr^2/V}}{4\pi i V}, \tag{18}$$

where

$$\frac{1}{V} = \frac{1}{A} - \frac{i}{R},$$

$$A = z_o + \xi^2/z_o, \qquad R = \xi + z_o^2/\xi,$$

and z_o is a constant.[13-15] To conform to Ziolkowski's example, Eq. (18) represents a pulse traveling to the right which is modulated by a plane wave moving to the left. With an appropriate weight function, it can be shown that the Ψ_k for all k form a complete set of basis functions, each with total energy proportional to $\int d^3\underline{r}\,|\Psi_k|^2 \to \infty$. Just as in the case of Fourier synthesis with plane waves, a general, finite-energy pulse may be obtained by superposing the various Ψ_k according to a weight function F(k), that is,

$$f(r,z,t) = \int_0^\infty dk\ \Psi_k(r,z,t)\ F(k)$$

$$= \frac{1}{4\pi i(z_0 + i\xi)} \int_0^\infty dk\ F(k)\ e^{-ks}, \tag{19a}$$

where

$$s = -i\eta + \frac{r^2}{z_0 + i\xi}. \tag{19b}$$

Equation (19a) indicates that f(r,z,t) is proportional to the Laplace transform of F(k).

ii) Modified Power-Spectrum Pulse -- Numerical Study

Ziolkowski has examined in detail the pulse corresponding to a modified power-spectrum (MPS):

$$F(k) = \begin{cases} 0, & 0 < k < b/\beta \\ 4\pi i\beta\ \dfrac{(\beta k - b)^{\alpha-1}\ e^{-a(\beta k - b)}}{\Gamma(\alpha)}, & k > b/\beta \end{cases} \tag{20a}$$

where $\Gamma(\alpha)$ is the Gamma function (Ref. 22) and a, α, and β are arbitrary constants. Upon substituting Eq. (20a) into Eq. (19) one obtains

$$f(r,z,t) = \left[\frac{1}{z_0 + i\xi}\ \frac{e^{-br^2/\beta(z_0+i\xi)}\ e^{ib\eta/\beta}}{[a + r^2/\beta(z_0+i\xi) - i\eta/\beta]^\alpha}\right]. \tag{20b}$$

The real part of this function defines the MPS pulse. The radial profile of the MPS pulse at the pulse center, $\xi = 0$, has the form

$$f(r,z) = \frac{1}{z_0} \frac{e^{ib\eta/\beta}}{(a + r^2/\beta z_0 - i\eta/\beta)^\alpha} e^{-br^2/\beta z_0}. \qquad (20c)$$

In the numerical studies the pulse was replicated by superposing the fields from a planar array of discrete points, each of which was driven by a function specified by the MPS form on some z = constant plane.[15] The parameters were: $a = 1.0$ cm, $b = 1.0 \times 10^{10}$ cm^{-1}, $\beta = 6.0 \times 10^{15}$, $z_0 = 1.667 \times 10^{-3}$, and $\alpha = 1$. The spectrum was approximately flat up to 200 GHz, becoming negligible beyond 15 THz. The pulse generated in this manner was propagated forward and compared with the exact form in Eq. (20b) at several locations along the z axis. The minimum radius of the array required to replicate the exact pulse form at 1, 10, 100, and 1,000 km was determined. From Ziolkowski's results we estimate the corresponding radii of the antenna to be approximately 0.5, 5, 50, and 500 m, respectively.

We shall examine these results by asking: What is the scale-length for diffraction of the MPS pulse? The pulse has a Gaussian radial profile, as indicated in Eq. (20c), with a width $w_0 = (\beta z_0/b)^{1/2} = 31.6$ cm and, therefore, Ziolkowski calculates a Rayleigh range $\pi w_0^2/\lambda = 0.21$ km for the 200 GHz component.[15] This, however, is not the appropriate scale-length for diffraction of the MPS pulse. The correct scale-length is given by $2\pi w_0 d/\lambda$, where the antenna dimension, d, always exceeds w_0. The point here is that the Rayleigh range based on the waist w_0, as calculated by Ziolkowski,[14,15] is only valid at the pulse center, $\xi = 0$. Away from the plane $\xi = 0$ the effective waist increases, as indicated by Eq. (20b), and the actual diffraction length is, therefore, longer than $\pi w_0^2/\lambda$. This explains why the pulse propagates further than the Rayleigh range defined in terms of w_o. To calculate the actual diffraction length, we note that the perpendicular wave number ($k_\perp$) spectrum given in Ref. 15 indicates that the smallest $k_\perp$ is on the order of $1/w_o$. Hence, an estimate for the diffraction angle is $\lambda/2\pi w_o$. The width of the radiation beam given by Eq. (3) can be written as $w = d + (\lambda/2\pi w_o)z$, where d is the radius of the array or "antenna." The scale-length for diffraction is then simply

$$Z_{MPS} = 2\pi w_o d/\lambda. \tag{21}$$

Note the similarity between the diffraction length in Eq. (21) and the scale-length for diffraction of the Bessel beam, $Z_B = 2\pi d/k_\perp \lambda$, derived in Section V, subsection ii). The resemblance is a reflection of the fact that in both cases the pulse energy is spread over the entire radius, d, of the aperture, which is much larger than the nominal waist of the beam, w_o.

According to Eq. (21) the larger the radius of the array is, the longer the distance of propagation of the pulse, consistent with the numerical results. From the numerical results, the ratio Z_{MPS}/d is equal to 2,000 which is the same as that given by Eq. (21) provided the frequency is 300 GHz. Since this frequency is well within the cutoff of the pulse spectrum, this constitutes a persuasive indication that the MPS pulse does not "defeat diffraction" as claimed by Ziolkowski.[14]

iii) Modified Power-Spectrum Pulse -- Experiment

Ziolkowski et al. have performed a water-tank experiment to demonstrate the properties of a MPS acoustic pulse.[16] The pulse was generated by a 6x6 cm^2 square array. The MPS pulse parameters were $a = 1.0$ m, $b = 600.0\ m^{-1}$, $\beta = 300.0$, $z_o = 4.5\times10^{4}$ m, and $\alpha = 1$. From these parameters one finds that the pulse width w_o is equal to 1.5 cm.

The experiment indicated that a Gaussian pulse with an initial width equal to 1.5 cm suffered a greater transverse spreading than the MPS pulse.

This experiment may be examined in the light of the discussion leading to Eq. (21). The expression in Eq. (21) gives the scale-length for the fall-off in the intensity of a pulse which is generated by an array (i.e., antenna) of radius d. Since the square array is 6x6 cm^2, we take the parameter d to be equal to 3 cm. Noting that the speed of sound in water is 1.5×10^3 m/s, the wavelength of the dominant frequency in the pulse, 0.6 MHz, is $\lambda = 2.5$ mm. From this, the actual diffraction scale-length Z_{MPS} is 1.1 m. This is in good agreement with the experimental observation that the MPS pulse propagated a distance of 1 m without significant spreading. Comparing the MPS pulse generated by a 6x6 cm^2 array with a Gaussian pulse having a waist of 1.5 cm is inappropriate. A Gaussian beam with spot size equal to the array radius used in the experiment would propagate a distance $\pi d^2/\lambda \simeq Z_{MPS}$; i.e. as far as the MPS pulse.

We note from Eq. (21) that, in general, a Gaussian beam with an appropriately curved wavefront and an initial spot size equal to the antenna dimension transfers nearly all the power onto a target of dimension w_o in a distance on the order of Z_{MPS}. Such a Gaussian beam, therefore, transfers more power on the target than the corresponding MPS pulse.

VII. Electromagnetic Bullets

In this section we shall discuss solutions of the wave equation which are confined to a finite region of space in the wave zone and are termed "electromagnetic bullets". We consider solutions of the wave equation

$$\left(\nabla^2 - c^{-2}\partial^2/\partial t^2\right)f(\underline{r},t) = -\rho(\underline{r},t), \tag{22}$$

where the source term $\rho(\underline{r},t)$ is assumed to be non-zero for a finite time interval $-T < t < T$. In this problem there are two cases of interest:

Case (a) is the direct source problem (initial value problem). In this case the solution for $t < T$ is given and the solution for $t > T$ is sought.

Case (b) is the inverse source problem. Here, the solution of the homogeneous wave equation for $|t| > T$ is known and one seeks the source term appropriate to this solution. This case is of particular interest since it would enable one to find the time-dependent source for a prescribed radiation field.

The following four subsections summarize the extensive research of Moses and Prosser on this subject. For a brief description of the properties of a bullet, the reader is referred to subsection iv).

i) Non-uniqueness of the Inverse Source Problem

In this subsection we indicate the reason for the non-uniqueness of the inverse source problem.[17] By making use of the eigenfunctions of the curl operator, the electromagnetic vector field wave equation may be solved along essentially the same lines as the one-dimensional problem. The discussion in this subsection is, therefore, confined to the one-dimensional wave equation to avoid the complications of multi-dimensional effects.

Let $f_+(x,t) = f(x,t)$ denote the solution of Eq. (22) for $t > T$, and $f_-(x,t) = f(x,t)$ denote the solution for $t < -T$. It is well-known that the solution of the source-free initial value problem for $t > T$ in terms of the values of the function $f_+(x,t)$ at $t = T$ and the "velocity" $(\partial/\partial t)f_+(x,t)$ at $t = T$ is expressible in terms of a propagator $G(x;t)$:

$$f_+(x,t) = \int dx' \; [G(x-x';t-T)\frac{\partial}{\partial t}f_+(x',t=T) + f_+(x',t=T)\frac{\partial}{\partial t}G(x-x';t-T)]. \tag{23a}$$

Similarly, the solution of the source-free final value problem for $t < -T$ in terms of $f_-(x,t)$ at $t = -T$ and $(\partial/\partial t)f_-(x,t)$ at $t = -T$ is given by

$$f_-(x,t) = \int dx' \; [G(x-x';t+T)\frac{\partial}{\partial t}f_-(x',t=-T) + f_-(x',t=-T)\frac{\partial}{\partial t}G(x-x';t+T)]. \tag{23b}$$

The propagator G can be written in terms of the Heaviside function η as follows

$$G(x;t) = \frac{1}{2}\,\mathrm{sgn}(t)\;\eta(c^2t^2 - x^2) = \frac{1}{2}\,[\eta(x+ct) - \eta(x-ct)]. \tag{24}$$

That is, G may be expressed as the difference between the advanced and the retarded Green functions. As a result, $f_+(x,t)$ is influenced only by points x at $t = T$ which lie in the backward light cone of the observation instant; similarly, $f_-(x,t)$ is influenced only by points x at $t = -T$ which lie in the forward light cone of the observation instant, as indicated in Fig. 5.

Let us now consider the effect of the source on the solution of the wave equation. We define two auxiliary functions,

$$\tilde{\rho}(k,t) = (2\pi)^{-1/2}\int_{-\infty}^{\infty} dx \;\rho(x,t)\; e^{-ikx}, \tag{25}$$

$$\tilde{f}(k,\sigma,t) = \tilde{f}(k,\sigma,-T)e^{-i\sigma c|k|(t+T)}$$

$$+ \frac{i\sigma}{2|k|} e^{-i\sigma c|k|t} \int_{-T}^{t} dt' \, \tilde{\rho}(k,t') \, e^{i\sigma c|k|t'}, \qquad (26)$$

where $\sigma = +1$ or -1 distinguishes the two directions of propagation along the x axis. Note that $\tilde{\rho}(k,t)$ is simply the spatial Fourier transform of $\rho(x,t)$. In terms of the two auxiliary functions, it is simple to show that

$$f(x,t) = (2\pi)^{-1/2} \sum_{\sigma} \int_{-\infty}^{\infty} dk \, \tilde{f}(k,\sigma,t) \, e^{ikx},$$

is a solution of the inhomogeneous wave equation in Eq. (22). The solutions for $t < -T$ and for $t > T$ are then given by

$$f_{\pm}(x,t) = (2\pi)^{-1/2} \sum_{\sigma} \int_{-\infty}^{\infty} dk \, e^{ikx} \, e^{-i\sigma c|k|(\pm T - t)} \, \tilde{f}(k,\sigma,\pm T). \qquad (27)$$

Equation (27) expresses the solution of the wave equation in terms $\tilde{f}$ evaluated at $\pm T$. This function is related to the source ρ by Eqs. (25) and (26). Equation (23), on the other hand, expresses the same solutions in terms of f and $(\partial/\partial t)f$ evaluated at $\pm T$. Hence, one would expect to be able to relate $\tilde{f}(k,\sigma,\pm T)$ with f and $(\partial/\partial t)f$ evaluated at $\pm T$. Indeed, the the formula connecting $\tilde{f}(k,\sigma,T)$ and f_+ is

$$\tilde{f}(k,\sigma,T) = (8\pi)^{-1/2} \int_{-\infty}^{\infty} dx \left[f_+(x,t=T) + i\frac{\sigma}{|k|} \frac{\partial}{\partial t} f_+(x,t=T)\right] e^{-ikx}, \qquad (28)$$

and $\tilde{f}(k,\sigma,-T)$ is obtained in terms of f_- by Fourier inversion of Eq. (27) evaluated at $t = -T$. Thus, in the direct source problem, $f_+(x,t)$ is obtained by specifying either $f_+(x,t)$ and $(\partial/\partial t)f_+(x,t)$ evaluated at $t = T$, or $f(x,-T)$ and $\rho(x,t)$.

We now turn to the inverse source problem. Inverse problems, in general, have been the subject of extensive research in many branches of physics. In our case we wish to determine the source from a knowledge of the field generated by that source. Supposing that $f_{\pm}(x,t)$ and T are known, we can determine $\tilde{f}(k,\sigma,\pm T)$ from Eqs. (27) and (28). Letting the upper limit of integration in Eq. (26) equal T, it appears that one can then obtain the temporal Fourier transform, $s(k,\omega)$, of $\tilde{\rho}(k,t)$, where

$$s(k,\omega) = (2\pi)^{-1/2} \int_{-T}^{T} dt' \; \tilde{\rho}(k,t') \; e^{i\omega t'}.$$

The source function is then given by

$$\rho(x,t) = (2\pi)^{-1} \int_{-\infty}^{\infty} dk \int_{-\infty}^{\infty} d\omega \; s(k,\omega) \; e^{ikx-i\omega t} \quad .$$

Thus, if $s(k,\omega)$ were known for all k and all ω, we could determine $\rho(x,t)$. However, referring to Eq. (26), we notice that $s(k,\omega)$ is only known for $\omega = \pm c|k|$, which is not sufficient to reconstruct $\rho(x,t)$. This complication is intimately connected with the <u>non-uniqueness</u> of the inverse problem.

Moses has shown that specification of the time-dependence of the source is sufficient to guarantee a unique solution.[17] As a concrete example, if $\rho(\underline{r},t) = \rho_e(\underline{r})h_e(t) + \rho_o(\underline{r})h_o(t)$, where h_e is an even function of t and h_o is an odd function of t, and both essentially arbitrary, then a complete solution of the inverse problem for $\rho_e(\underline{r})$ and $\rho_o(\underline{r})$ is possible. It must be stressed, however, that this assumed form for the source function is a sufficient but not necessary condition for the solvability of the inverse problem.

Without going into details we cite the example given in Ref. 17. For simplicity taking the time dependence to be of the form $h_e(t) = \delta(t)$, $h_o(t) = \delta'(t)$, where $' = d/dt$, and assuming the field to be of the form

$$f_+(x,t) = \sin[k(x - ct)], \qquad -a < x - ct < a, \qquad ka = n\pi,$$

the source function is found to be given by

$$\rho(x,t) = -[k\ \delta(t) \cos(kx) - c^{-1}\delta'(t) \sin(kx)], \qquad -a < x < a.$$

Note that in this case the source is confined to a finite region of space, which is an important attribute for any physically realizable source function. {We should point out that the source function given by Moses is erroneous due to a sign error in evaluating the Fourier transform of $h_o(t)$ [his Eq. (2.36′)].}

ii) <u>Solution of the Three-Dimensional Wave Equation in the Wave Zone</u>

The general solution of the source-free three-dimensional wave equation is[18]

$$f(\underline{r},t) = (2\pi)^{-3/2} \sum_{\sigma} \int d^3\underline{k}\ e^{i\underline{k}\cdot\underline{r} - i\sigma ckt}\ \tilde{f}(\underline{k},\sigma), \tag{29}$$

where $\sigma = \pm 1$, and $k = |\underline{k}|$. Making use of the method of stationary phase, it can be shown that

$$\lim_{r\to\infty} e^{i\underline{k}\cdot\underline{r}} = \frac{2\pi i}{kr\ \sin\theta} \Big[-e^{ikr}\delta(\theta - \theta_x)\delta(\phi - \phi_x) + e^{ikr}\delta(\theta - \theta_x')\delta(\phi - \phi_x') \Big], \tag{30}$$

where (θ_x, ϕ_x) are the angles in the cone along +z axis, and θ_x', ϕ_x' are the angles in the cone along -z axis.[22] We shall define cones more precisely in the following. Upon substituting Eq. (30) into Eq. (29), the field in the wave zone is found to be given by

$$f(\underline{r},t) = (8\pi)^{-1/2} r^{-1} \mathrm{Im} \int_0^\infty dk \left[e^{ik(r-ct)} \tilde{f}(k,\theta_x,\phi_x) - e^{ik(r+ct)} \tilde{f}(k,\theta_x',\phi_x') \right]. \tag{31}$$

Remarkably, Eq. (31) shows that the general solution of the three-dimensional wave equation in the wave zone is, apart from the factor $1/r$, a superposition of one-dimensional wave motion, expressed as functions of $r - ct$ and $r + ct$. Moreover, if initially $f(\underline{r},t)$ is confined to a given solid angle, $\tilde{f}(k,\theta,\phi)$ will be significant for $\underline{k}$ lying within that angle and, from Eq. (31), the solution in the wave zone will also be confined to the same angle. For the purposes of interpretation it is convenient to consider propagation in cones, as indicated in Fig. 6. In particular, an electromagnetic field in a cone is defined as one that is completely confined to a cone in the wave zone.

iii) Exact Solution of the Wave Equation from the Solution in the Wave Zone (Radon Transforms)

The purpose of this subsection is to point out that, given the solution of the wave equation in the wave-zone region, it is possible to determine the solution everywhere.[18,19] In particular, one seeks the initial conditions $f(\underline{r},t)$ and $(\partial/\partial t)f(\underline{r},t)$ at $t = T$. This is referred to as the inverse initial value problem.

The solution of the inverse initial value problem is discussed in Ref. 18 for a particularly simple case. A systematic treatment of the general problem is possible by using Radon transforms.[19]

The Radon transform $F(k,\hat{n})$ of a function $f(\underline{r})$ is obtained by integrating f over all planes $\underline{r}.\hat{n}$ = const.

$$F(k,\hat{n}) = \int d^3\underline{r}\ f(\underline{r})\ \delta(\underline{r}\cdot\hat{n} - k),$$

where $\hat{n}$ is a unit vector.[24] The usual Radon transform is defined as an integral over planes whose normals vary over a unit sphere. In general, the function $f(\underline{r})$ defines some internal distribution (such as density) of an object and $F(k,\hat{n})$ is the projected distribution, or the profile, of the object on the plane $\underline{r}.\hat{n}$ = constant. The Radon transform is a very useful tool in image reconstruction from projections, with applications in computer-assisted tomography (CAT)-scan, radio astronomy, remote sensing, etc.

A refinement of the usual definition of the Radon transform shows that only the transform over a hemisphere, which may consist of disjointed parts, is sufficient to reconstruct the original function. It can then be shown that the task of obtaining an exact solution of the three-dimensional wave equation from the solution in the wave zone reduces to taking the inverse of the refined Radon transform of the solution in the wave zone.

From Eq. (31) it is known that in the wave zone the solution of the wave equation is, apart from a factor $1/r$, a function of only $r-ct$ or $r+ct$, representing propagation along rays confined to a cone. The field in the wave zone, therefore, defines the range of the unit vector $\hat{n}$ and the amplitude. This information is essentially equivalent to knowing the projections in different directions. The exact field may then be reconstructed from the set of projections.

iv) Example of a Bullet

We close Section VII by discussing an explicit example of a bullet which is a solution of the scalar wave equation.[20] An example of an electromagnetic bullet is given in Ref. 20.

A bullet which is confined to a finite volume in the wave-zone is given by

$$f(\underline{r},t) = \eta(\sigma - \theta)\, [\eta(r-a-ct) - \eta(r-b-ct)]/r, \qquad r \to \infty, \tag{32}$$

where η is the Heaviside function, a and b, with $b > a$, denote the boundaries of the bullet along the radius, and 2σ is the vertex angle of the cone containing the bullet. Note that this solution is causal and of finite energy, and has a form which is consistent with the remarks following Eq. (31). It represents a packet of energy "shot" through a cone whose axis coincides with the z axis.

This solution can be easily verified by letting $f = g(r,\theta,t)/r$ and noting that

$$\left(\nabla^2 - c^{-2}\frac{\partial^2}{\partial t^2}\right)f = \left(\frac{\partial^2}{\partial r^2} - c^{-2}\frac{\partial^2}{\partial t^2}\right)g + \frac{1}{r^2\sin\theta}\frac{\partial}{\partial\theta}\left(\sin\theta\frac{\partial}{\partial\theta}\right)g.$$

Assuming $g(r,\theta,t) = h(r-ct-r_0)Y(\theta)$, one finds

$$\left(\nabla^2 - c^{-2}\frac{\partial^2}{\partial t^2}\right)f = \frac{h}{r^2\sin\theta}\frac{d}{d\theta}\left(\sin\theta\frac{d}{d\theta}Y\right), \tag{33}$$

which tends to zero for all continuous $Y(\theta)$ as $r \to \infty$. For the case when $Y(\theta) = \eta(\sigma - \theta)$, we let $-dY/d\theta = \exp[-(\sigma-\theta)^2/2\Delta^2]/(2\pi)^{1/2}\Delta$, with $\Delta \to 0$. Note that as $\Delta \to 0$, $dY/d\theta \to -\delta(\sigma-\theta) = d\eta(\sigma-\theta)/d\theta$. Upon substituting this form into Eq. (33), we notice that as Δ is made to approach zero, r must increase indefinitely in order for the right-hand side of Eq. (33) to approach zero. This shows very clearly that Eq. (32) is indeed a solution in the wave zone.

The spot size may be defined by:

$$r_s^2 = \int dr\,d\theta\,d\phi\; f\; r^2\sin\theta\,(2r\sin\theta)^2 \Big/ \int dr\,d\theta\,d\phi\; f\; r^2\sin\theta, \tag{34}$$

where $2r\sin\theta$ is the width of a cone of half-angle θ. Substituting Eq. (32) into Eq. (34), one obtains

$$r_s \to [(8 - 9\cos\sigma + \cos 3\sigma)/3(1 - \cos\sigma)]^{1/2} ct, \qquad t \to \infty, \tag{35}$$

indicating a linear increase with time for the spot size, as in the case of the Gaussian pulse in Eq. (14b), although the constants of proportionality are different. We mention in passing that the solutions given by Moses and Prosser are distinguished from the other solutions reviewed here by not having an explicit dependence on the frequency or the wave number.

As mentioned in the previous subsection, to obtain the exact solution everywhere one has merely to evaluate the inverse Radon transform of the solution in the wave zone, Eq. (32). Since the derivation is lengthy we shall simply quote the result The exact solution is given by

$$f(\underline{r},t) = f_a(\underline{r},t) - f_b(\underline{r},t), \tag{36a}$$

where

$$f_a(\underline{r},t) = \eta(\sigma-\theta)\ \{\eta[a+ct-r\cos(\theta-\sigma)] - \eta(a+ct-r)\}/r$$

$$+ \nu_a\{\eta[a+ct-r\cos(\theta+\sigma)] - \eta[a+ct-r\cos(\theta-\sigma)]\}/\pi r, \tag{36b}$$

with

$$\nu_a = \cos^{-1}[(\cos\sigma - \cos\beta_a\cos\theta)/\sin\beta_a\sin\theta], \qquad 0 < \nu_a < \pi,$$

and

$$\beta_a = \cos^{-1}[(a+ct)/r], \qquad 0 < \beta_a < \pi/2,$$

and where $f_b(\underline{r},t)$ is identical to $f_a(\underline{r},t)$ except that a is replaced by b.

The field in Eq. (36) is identically zero for all r downstream of the bullet, i.e., for all $r < a + ct$. The wave-zone limit is obtained by taking $r, t \to \infty$. Then, since Eq. (36) corresponds to propagation in the positive cone (Fig. 6), taking $r - ct$ = constant Eq. (32) is recovered. The requirement $r - ct$ = constant is equivalent to observing the bullet in a co-moving frame. Close to the origin the exact solution in Eq. (36) spreads out of the cone significantly. However, in the wave zone the solution is confined to the cone and is independent of the angle θ therein. Finally, it has been shown in Ref. 20 that the difference between the exact solution in Eq. (36) and the wave-zone solution in Eq. (32) becomes small quite rapidly as r, ct increase, with $r - ct$ held fixed.

In principle, one can now use the inverse source method to determine the sources that lead to the bullet described by Eq. (32). To our knowledge, however, this computation has yet to be performed.

VIII. Summary and Concluding Remarks

The motivation for much of the research reviewed herein stems from the need to propagate a beam of radiation over long distances without an appreciable decrease in the intensity. Possible applications would include: power beaming, advanced radar, laser acceleration of particles and directed energy sources. This need has led to a great deal of interest in such fundamental subjects as diffraction and new solutions of the wave equation.

It has been reiterated that the physical basis for diffraction of waves is the well-known relation $\Delta k_i \Delta x_i \approx 1$, for $i = 1,2,3$. By virtue of this, it is simple to determine the scale length for the diffractive spreading of a beam with an arbitrary transverse profile. Thus, a knowledge of the spectrum is sufficient to determine the maximum propagation distance of the beam. Since diffraction is unavoidable, by concentrating the energy in the high frequencies one can only delay the spreading of the beam.

Four examples of the research effort on the subject of beam propagation have been reviewed herein. The conclusions are as follows.

i) Electromagnetic Missiles

Experiment indicates that a suitably tailored pulse-shape can be designed to have an energy decay rate limited by the highest frequencies present in the pulse. This is fully consistent with our understanding of diffraction.

ii) Bessel Beams

It is shown that as far as propagation is concerned Bessel beams are not "resistant to the diffractive spreading commonly associated with all wave propagation". These beams propagate no further than Gaussian beams or plane waves with the same transverse dimensions.

iii) Electromagnetic Directed Energy Pulse Trains

The diffractive properties of the pulse form studied most intensively under this general heading are described by diffraction theory. These pulse trains do not "defeat diffraction".

iv) Electromagnetic Bullets

Given a radiation wave packet in the wave-zone which is confined to a suitable solid angle and extends over a finite radial extent, one can determine the source required to generate the wave packet. As of this writing, however, this problem has not been solved for a practical case.

Acknowledgment

This work was supported by the Office of Naval Research and the Department of Energy.

Appendix

The purpose of this appendix is to examine the transition from the Fresnel to the Fraunhofer region for a clipped Bessel beam and a clipped Gaussian beam within the context of the Huygens-Fresnel approximation.[25] The clipping is assumed to be caused by a finite-size aperture.

In the case of the Bessel beam the field distribution at the aperture has the form $u(r,z=0) = J_o(k_\perp r)$ within a circular aperture of radius d. Making use of Eq. (6) the amplitude at a point on the axis of symmetry is given by

$$\psi \propto z^{-1}\int_o^d dr'\ r'\ J_o(k_\perp r')\ e^{ikr'^2/2z}. \tag{A1}$$

The limit $k_\perp = 0$ corresponds to the case of plane waves incident on a circular aperture, as in Section III. The intensity, given by Eq. (9), falls off monotonically for $z > Z_p$, where

$$Z_p = 2\pi d^2/\lambda. \tag{A2}$$

For $k_\perp > 0$, the oscillatory behavior of the Bessel function in Eq. (A1) tends to phase mix the integrand, effectively reducing the upper limit of the integration. Consequently, the boundary of the Fresnel region, beyond which the radiation appears to be emitted essentially from a point source, is reached prior to $Z_p = 2\pi d^2/\lambda$.

Since there is no simple analytical approximation to the integral in Eq. (A1), consider the case of a cosine beam $u(x,y,z=0) = \cos(k_x x)\cos(k_y y)$, which is the cartesian equivalent of a Bessel beam. The aperture is a rectangular opening in the x-y plane defined by $\{(x,y),\ |x| < X,\ |y| < Y\}$. In terms of

$$\xi_{\pm} = (k/2z)^{1/2}(X \pm k_x z/k), \qquad (A3)$$

the amplitude on the z axis has the form $\psi \propto I_x I_y$, where

$$I_x = e^{-ik_x^2 z/2k}[C(\xi_+) + iS(\xi_+) + C(\xi_-) + iS(\xi_-)], \qquad (A4)$$

and

$$S(t) = (2/\pi)^{1/2}\int_0^t dt \sin t^2, \qquad C(t) = (2/\pi)^{1/2}\int_0^t dt \cos t^2,$$

are the Fresnel integrals.[22] The expression for I_y is obtained from that for I_x by making the replacements $k_x \rightarrow k_y$, $X \rightarrow Y$.

We are interested in the intensity well within a nominal Fresnel region defined by the width of the aperture

$$z << k(X^2, Y^2)/2, \qquad (A5)$$

but sufficiently far from the aperture so that the radiation diffracted from one edge can reach the z axis:

$$z \simeq k(X/k_x, Y/k_y). \qquad (A6)$$

Taking the appropriate limits of the Fresnel integrals, the intensity is $I \simeq I_0/16$, where I_0 is the intensity at the diffracting aperture. This analysis indicates that Eq. (A6) defines the boundary of the true Fresnel region. The terms proportional to $\pm k_x z/k$ in Eq. (A3) represent propagation at an angle $\pm \sin^{-1}(k_x/k)$ to the z axis. As a consequence the drop in intensity characterizing the transition to the Fraunhofer region takes place at the location indicated by Eq. (A6) rather than by the right hand side of Eq. (A5).

Returning to the Bessel beam with $d \gg 1/k_\perp$, in the region of significant phase mixing in the integrand of Eq. (A1) the Bessel function has the asymptotic form[22] $J_o(z) \sim (2/\pi z)^{1/2}\cos(z - \pi/4)$. Substituting this into Eq. (A1) and comparing the phases, it follows that the Fraunhofer region for the Bessel beam commences at $Z_B \simeq 2\pi d/k_\perp\lambda$. From the definition of Z_P in Eq. (A2) we note that $Z_B/Z_P = 1/k_\perp d \ll 1$ for the experimental parameters in Ref. 11. Thus, we see that a Bessel beam is not optimum as far as the diffractive fall-off of the intensity is concerned.

For the Gaussian beam, substituting $u(r)\exp(-r^2/w_o^2)$ into Eq. (6) and performing the integral, the intensity on the axis of symmetry is found to be given by

$$I \propto \frac{1 + e^{-2(d/w_o)^2} - 2e^{-(d/w_o)^2}\cos(kd^2/2z)}{1 + (z/Z_R)^2}, \tag{A7}$$

where Z_R is the Rayleigh range defined in Eq. (1). For the parameters in Ref. 11, $d/w_o \gg 1$, and the scale-length for the intensity to drop to a quarter of its initial value is on the order of $2Z_R$, as in Eq. (4c). This same scale-length is roughly applicable to the case of a wider Gaussian beam with $w_o \simeq d$. For an infinitely wide beam, $w_o \to \infty$, and Eq. (A7) goes over to the case of plane waves, Eq. (9).

For the off axis intensity of the cosine beam we limit the discussion to the case where the observation point is an integral number of half periods off of the z axis. In analogy with Eq. (A3) we define

$$\xi_\pm = (k/2z)^{1/2}[X + (k_x z/k - n_x\pi/k_x)],$$

$$\eta_\pm = (k/2z)^{1/2}[X + (k_x z/k + n_x\pi/k_x)],$$

where $n_x\pi/k_x$, with n_x an integer, is the x-coordinate of the observation point. We assume $n_x\pi/k_x < X$. In terms of these variables, the amplitude has the form $\psi \propto I_x I_y$, where

$$I_x \propto [C(\xi_+) + iS(\xi_+) + C(\xi_-) + iS(\xi_-) + C(\eta_+) + iS(\eta_+) + C(\eta_-) + iS(\eta_-)], \tag{A8}$$

where C and S are the Fresnel integrals defined earlier and the expression for I_y is obtained from that for I_x by making the substitution $k_x \to k_y$, $X \to Y$, and $n_x \to n_y$.

For plane waves ($k_{x,y} \to 0$) and on the symmetry axis ($n_{x,y} \to 0$) the transition from the oscillatory to the monotonically falling behavior of the Fresnel integrals in Eq. (A8) takes place at $z \approx k(X^2,Y^2)/2$. This marks the boundary between the Fresnel and Fraunhofer regions. For the cosine beam and on the symmetry axis ($n_{x,y} \to 0$) Eq. (A8) reduces to Eq. (A4) and hence Eq. (A6) defines the boundary between the two regions. Away from the symmetry axis ($n_{x,y} > 0$) the behavior is somewhat more complicated. On the aperture, $z = 0$, and $\xi_\pm$, $\eta_\pm \to \infty$, whence $I_x = 2(1 + i)$. For z sufficiently large so that $0 < \eta_- < 1$, but ξ_+, ξ_-, $\eta_+ >> 1$, the last two terms in Eq. (A8) are small and $I_x \to 3(1 + i)/2$. From the definition of η_- we note that as the observation point approaches the edge of the aperture ($n_x\pi/k_x \to X$) this reduction in the value of I_x is obtained at smaller values of z, according to the formula $z = k(X - n_x\pi/k_x)k_x$. Figure 7, which plots $|I_x|^2$ as a function of z, confirms this behavior for parameters similar to that in Ref. 11.

References

1. A. E. Siegman, An Introduction to Lasers and Masers, (McGraw-Hill, New York, 1971), chap. 8.
2. G. Toraldo di Francia, Nuovo Cimento, Suppl. 9, 426 (1952).
3. W. T. Welford, Optics, (Oxford University Press, New York, 1981), chap. 3.
4. C. J. Bouwkamp, Rep. Prog. Phys. 17, 35 (1954).
5. J. N. Brittingham, J. Appl. Phys. 54, 1179 (1983).
6. P. A. Belanger, J. Opt. Soc. Am. A1, 723 (1984).
7. T. T. Wu, J. Appl. Phys. 57, 2370 (1985).
8. T. T. Wu, H. M. Shen, and J. M. Myers, in Proceedings of the SPIE Conference 1061 on Microwave and Particle Beam Sources and Directed Energy Concepts, Los Angeles 1989, edited by H. E. Brandt (Society of Photo-Optical Instrumentation Engineers, Bellingham, WA, 1989), p. 370.
9. H. M. Shen, in Proceedings of the SPIE Conference 873 on Microwave and Particle Beam Sources and Propagation, Los Angeles 1988, edited by N. Rostoker (Society of Photo-Optical Instrumentation Engineers, Bellingham, WA, 1988), p. 338.
10. J. Durnin, J. Opt. Soc. Am. A4, 651 (1987).
11. J. Durnin, J. J. Miceli and J. H. Eberly, Phys. Rev. Lett. 58, 1499 (1987).
12. J. Durnin, J. J. Miceli and J. H. Eberly, Opt. Lett. 13, 79 (1988).
13. R. W. Ziolkowski, J. Math. Phys. 26, 861 (1985).
14. R. W. Ziolkowski, in Ref. 9, p. 312.
15. R. W. Ziolkowski, Phys. Rev. A 39, 2005 (1989).

16. R. W. Ziolkowski, D. K. Lewis and B. D. Cook, Phys. Rev. Lett. 62, 147 (1989).

17. H. E. Moses, J. Math. Phys. 25, 1905 (1985).

18. H. E. Moses and R. T. Prosser, IEEE Trans. Antennas Propag. AP-34, 188 (1986).

19. H. E. Moses and R. T. Prosser, Proc. R. Soc. Lond. A 422, 343 (1989); Proc. R. Soc. Lond. A 422, 351 (1989).

20. H. E. Moses and R. T. Prosser, to be published in the J. of the Society for Industrial and Applied Mathematics, SIAM J. Appl. Math. (1990).

21. J. D. Jackson, Classical Electrodynamics, (Wiley, New York, 1975), chap. 9.

22. I. S. Gradshteyn and I. M. Ryzhik, Table of Integrals, Series, and Products (Academic, San Diego, 1980).

23. I. W. Kay and H. E. Moses, Nuovo Cimento 22, 689 (1961).

24. S. R. Deans, The Radon Transform and Some of Its Applications, (Wiley, New York, 1983).

25. W. H. Southwell, J. Opt. Soc. Am. 71, 7 (1981).

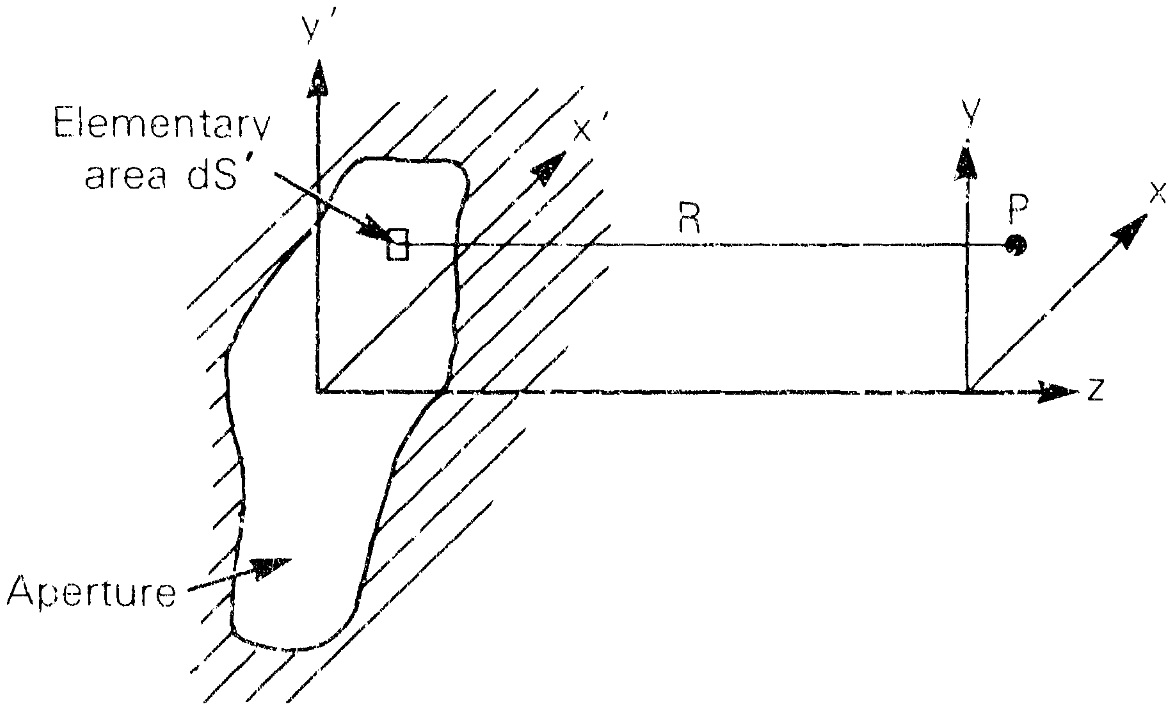

Figure 1

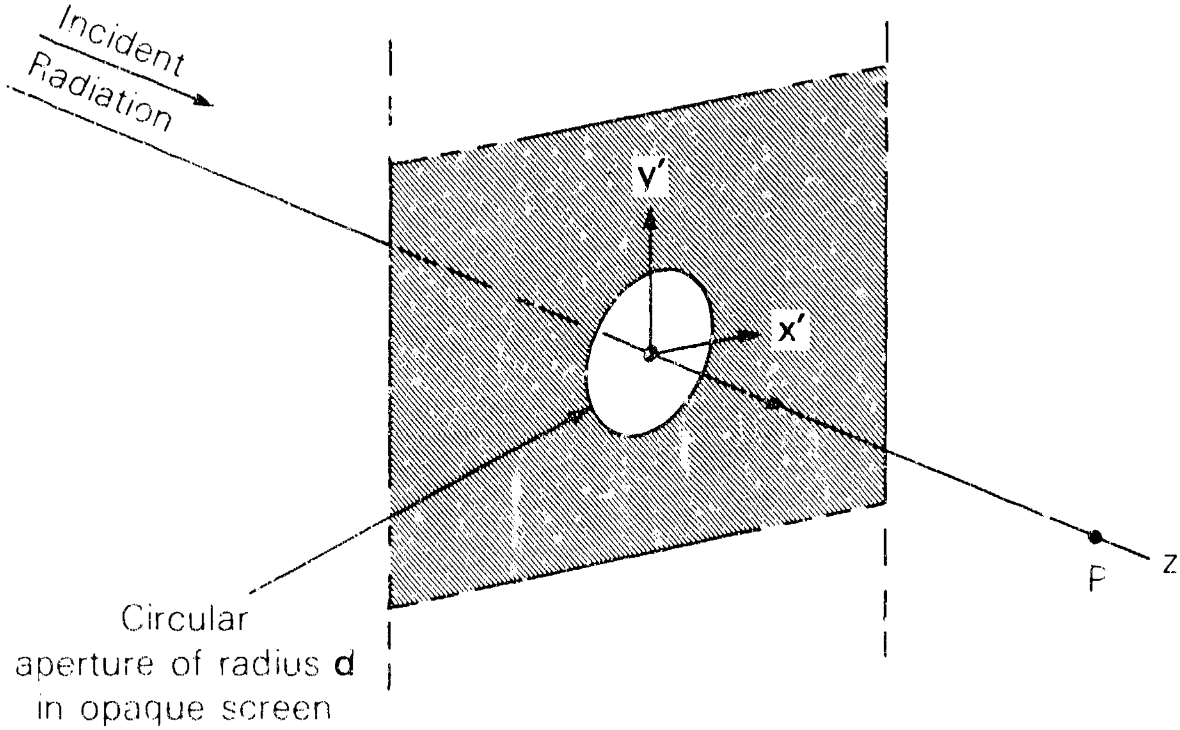
Incident
Radiation
y′
x′
P
z
Circular
aperture of radius d
in opaque screen

Figure 2

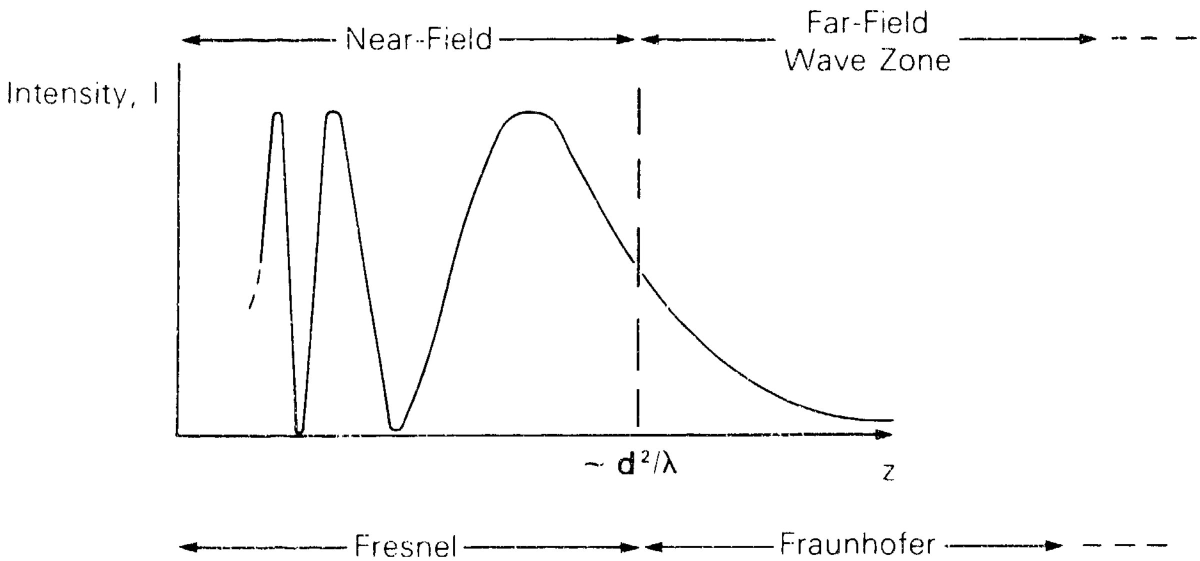
Near-Field
Far-Field
Wave Zone
Intensity, I
~ d²/λ
z
Fresnel
Fraunhofer

Figure 3

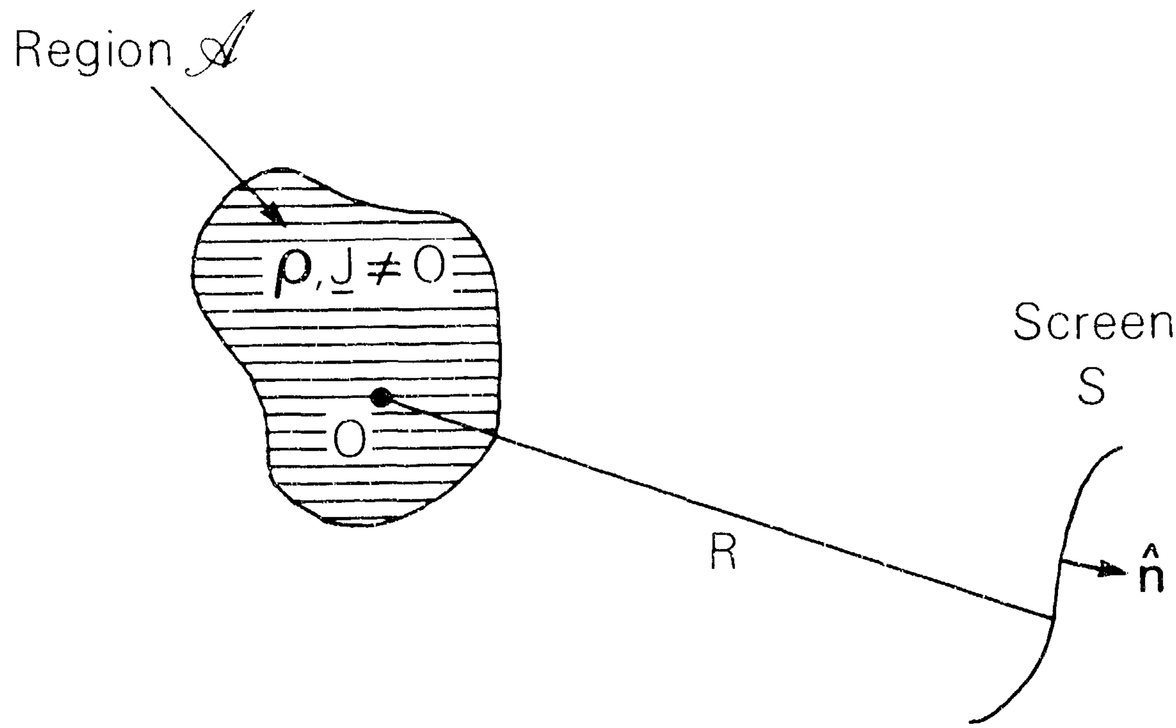

Figure 4

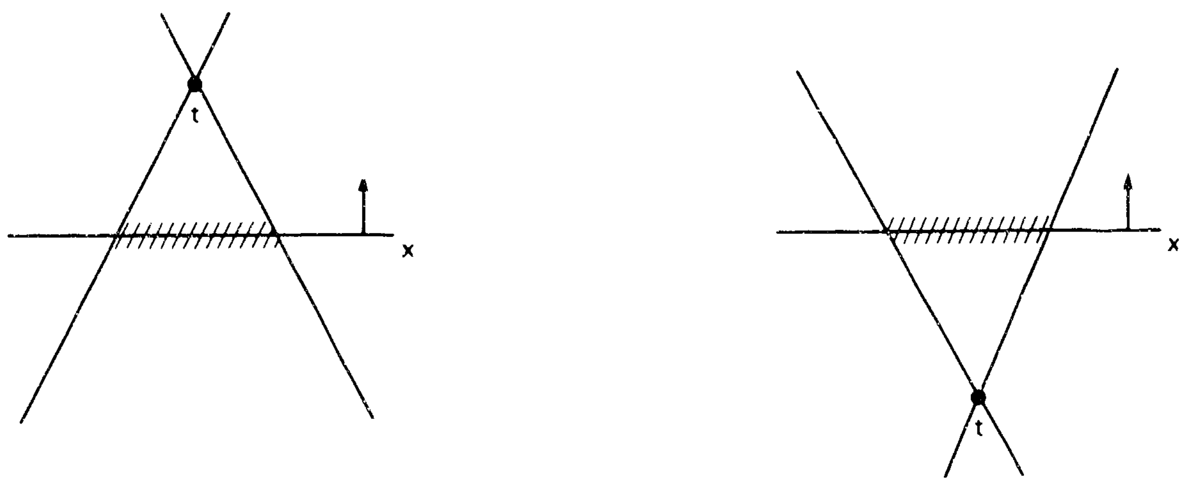

BACKWARD LIGHT CONE FORWARD LIGHT CONE

CAUSAL PROPAGATION

Figure 5

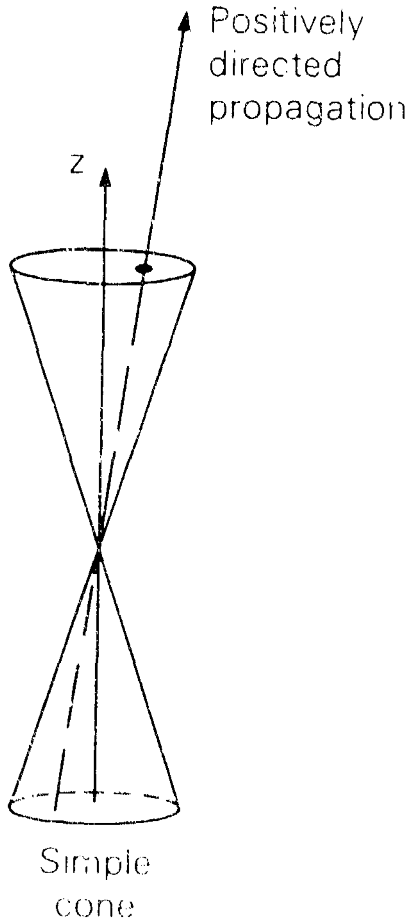

Figure 6

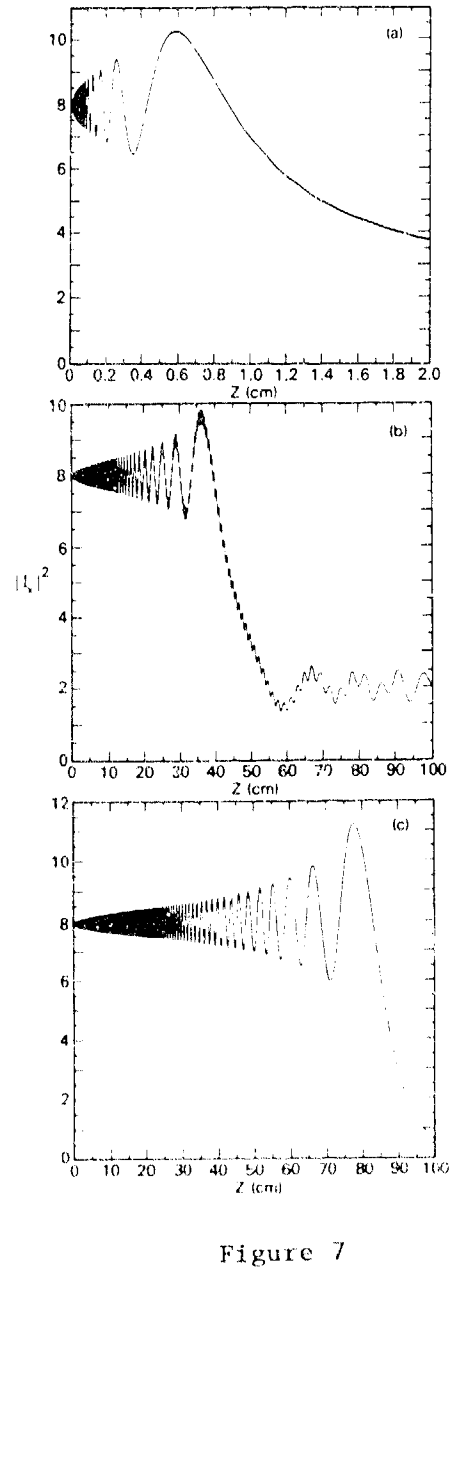

Figure 7

DISTRIBUTION LIST

Naval Research Laboratory
4555 Overlook Avenue, S.W.
Washington, DC 20375-5000

Attn: Code 1000 - Commanding Officer, CAPT John J. Donegan, Jr.
1001 - Dr. T. Coffey
1005 - Head, Office of Management & Admin.
1005.1-Deputy Head, Office of Management & Admin.
1005.6-Head, Directives Staff
1200 - CAPT R. W. Michaux
1201 - Deputy Head, Command Support Division
1220 - Mr. M. Ferguson
2000 - Director of Technical Services
2604 - NRL Historian
3000 - Director of Business Operations
4000 - Dr. W. R. Ellis
0124 - ONR
4600 - Dr. D. Nagel
4603 - Dr. W. W. Zachary
4700 - Dr. S. Ossakow (26 copies)
4707 - Dr. W. M. Manheimer
4730 - Dr. R. Elton
4770 - Dr. G. Cooperstein
4780 - Dr A. W. Ali
4790 - Dr. C. M. Tang
4790 - Dr. G. Joyce
4790 - Dr. M. Lampe
4790 - Dr. Y. Y. Lau
4790 - Dr. A. Ting
4790 - Dr. E. Esarey
4790 - Dr. J. Krall
4790A- B. Pitcher (20 copies)
4790 - Dr. P. Sprangle
4793 - Dr. W. Black
4793 - Dr. S. Gold
4793 - Dr. D. L. Hardesty
4793 - Dr. A. K. Kinkead
4794 - Dr. A. W. Fliflet
4794 - Dr. M. Rhinewine
4795 - Dr. C. A. Kapetanakos
4795 - Dr. J. Mathew
5700 - Dr. L. A. Cosby
5745 - Dr. J. Condon
6840 - Dr. S. Y. Ahn
6840 - Dr. A. Ganguly
6840 - Dr. R. K. Parker
6843 - Dr. R. H. Jackson
6843 - Dr. N. R. Vanderplaats
6843 - Dr. C. M. Armstrong
6875 - Dr. R. Wagner
2628 - Documents (22 copies)
2634 - D. Wilbanks

NOTE: Every name listed on distribution gets one copy except for those where extra copies are noted.

Dr. R. E. Aamodt
Lodestar Research Corp.
2400 Central Ave., P-5
Boulder, CO 80306-4545

Dr. J. Adamski
Boeing Aerospace Company
P.O. Box 3999
Seattle, WA 98124

Dr. T. M. Antonsen
University of Maryland
College Park, MD 20742

Assistant Secretary of the
Air Force (RD&L)
Room 4E856, The Pentagon
Washington, D.C. 20330

Dr. W. A. Barletta
Lawrence Livermore National Lab.
P. O. Box 808
Livermore, CA 94550

Dr. W. Becker
Univ. of New Mexico
Institute for Mod. Opt.
Albuquerque, NM 87131

Dr. Robert Behringer
9342 Balcon Ave.
Northridge, CA 91325

Dr. G. Bekefi
Mass. Institute of Tech.
Room 36-213
Cambridge, MA 02139

Dr. Steven V. Benson
Physics Building
Duke University
Durham, NC 27706

Dr. I. B. Bernstein
Mason Laboratory
Yale University
400 Temple Street
New Haven, CT 06520

Dr. Amitava Bhattacharjee
Columbia University
S. W. Mudd 210
Dept. of Applied Phys.
New York, NY 10027

Dr. Anup Bhowmik
Rockwell International/Rocketdyne Div.
6633 Canoga Avenue, FA-40
Canoga Park, CA 91304

Dr. G. Bourianoff
1901 Rutland Drive
Austin, TX 78758

Dr. Charles Brau
Vanderbilt University
Nashville, TN 37235

Dr. R. Briggs
SSC Laboratory
Stoneridge Office Park
2550 Beckleymeade Ave.
Suite 260
Dallas, TX 75237

Prof. William Case
Dept. of Physics
Grinnell College
Grinnell, IA 50112

Dr. R. Center
Spectra Tech., Inc.
2755 Northup Way
Bellevue, WA 98004

Dr. K. C. Chan
Los Alamos National Laboratory
P. O. Box 1663
Los Alamos, NM 87545

Prof. Frank Chen
School of Eng. & Applied Sciences
Univ. of Calif. at Los Angeles
7731 K Boelter Hall
Los Angeles, CA 90024

Dr. S. Chen
MIT Plasma Fusion Center
NW16-176
Cambridge, MA 01890

Dr. D. P. Chernin
Science Applications Intl. Corp.
1720 Goodridge Drive
McLean, VA 22102

Dr. William Colson
Naval Postgraduate School
Physics Dept.
Monterey, CA 93940

Dr. Richard Cooper
Los Alamos National Scientific Laboratory
P.O. Box 1663
Los Alamos, NM 87545

Dr. R. A. Cover
Rockwell International/Rocketdyne Div.
6633 Canoga Avenue, FA-38
Canoga Park, CA 91304

Dr. Bruce Danly
MIT
NW16-174
Cambridge, MA 02139

Dr. R. Davidson
Plasma Fusion Center
Mass. Institute of Tech.
Cambridge, MA 02139

Dr. John Dawson
Physics Department
University of California
Los Angeles, CA 90024

Dr. David A. G. Deacon
Deacon Research
2440 Embarcadero Road
Palo Alto, CA 94303

Dr. Philip Debenham
Center for Radiation Research
National Bureau of Standards
Gaithersburg, MD 20899

Director
National Security Agency
Fort Meade, MD 20755
ATTN: Dr. Richard Foss, A42
Dr. Thomas Fandel, A243
Dr. Robert Madden, R/SA

Director of Research (2 copies)
U. S. Naval Academy
Annapolis, MD 21402

Dr. A. Drobot
Science Applications Intl. Corp.
1710 Goodridge Road
McLean, VA 22102

Dr. Dwight Duston
SDIO/IST
The Pentagon
Washington, DC 20301-7100

Dr. Luis R. Elias
Creol-FEL Research Pavillion
Suite 400
12424 Research Parkway
Orlando, FL 32826

Dr. C. James Elliott
X1-Division, M.S. 531
Los Alamos Natl. Scientific Lab.
P. O. Box 1663
Los Alamos, NM 87545

Dr. Anne-Marie Fauchet
Brookhaven National Laboratories
Associated Universities, Inc.
Upton, L.I., NY 11973

Dr. R. Gajewski
Div. of Advanced Energy Projects
U. S. Dept of Energy
Washington, DC 20545

Dr. J. Gallardo
Brookhaven National Laboratory
Associated Universities, Inc.
Upton, L.I., NY 11973

Dr. B. B. Godfrey,
Chief Scientist
WL/CA
Kirtland AFB, NM 87117-6008

Dr. John C. Goldstein, X-1
Los Alamos Nat'l. Scientific Lab.
P.O. Box 1663
Los Alamos, NM 87545

Dr. V. L. Granatstein
Dept. of Electrical Engineering
University of Maryland
College Park, MD 20742

Dr. K. Halbach
Lawrence Berkeley Laboratory
University of California, Berkeley
Berkeley, CA 94720

Dr. R. Harvey
Hughes Research Laboratory
3011 Malibu Canyon Road
Malibu, CA 90265

Prof. Herman A Haus
Mass. Institute of Technology
Rm. 36-351
Cambridge, MA 02139

Dr. B. Hui
Defense Advanced Research Projects Agency
1400 Wilson Blvd.
Arlington, VA 22209

Prof. V. Jaccarino
Univ. of Calif. at Santa Barbara
Santa Barbara, CA 93106

Dr. B. Carol Johnson
Ctr. for Radiation Research
National Inst. of Standards and Tech.
Gaithersburg, MD 20899

Dr. Ron Johnson
Ctr. for Radiatiuon Research
Natl. Inst. of Standards and Tech.
Gaithersburg, MD 20899

Dr. Shayne Johnston
Physics Department
Jackson State University
Jackson, MS 39217

Dr. R. A. Jong
Lawrence Livermore National Laboratory
P. O. Box 808/L626
Livermore, CA 94550

Dr. Howard Jory
Varian Associates, Bldg. 1
611 Hansen Way
Palo Alto, CA 94303

Dr. C. Joshi
University of California
Los Angeles, CA 90024

Dr. K. J. Kim, MS 101
Lawrence Berkeley Lab.
Rm 223, B-80
Berkeley, CA 94720

Dr. Brian Kincaid
Lawrence Berkeley Laboratory
University of California, Berkeley
Berkeley, CA 94720

Prof. N. M. Kroll
Department of Physics
B-019, UCSD
La Jolla, CA 92093

Dr. Thomas Kwan
Los Alamos National Scientific
Laboratory, MS608
P. O. Box 1663
Los Alamos, NM 87545

Dr. J. LaSala
Physics Dept.
U. S. M. A.
West Point, NY 10996

Dr. Michael Lavan
U.S. Army Strategic Def. Command
ATTN: Code CSSD-H-D
P. O. Box 1500
Huntsville, AL 35807-3801

Dr. B. Levush
Dept. of Physics & Astronomy
University of Maryland
College Park, MD 20742

Dr. Anthony T. Lin
Dept. of Physics
University of California
Los Angeles, CA 90024

Dr. Chuan S. Liu
Dept. of Physics & Astronomy
University of Maryland
College Park, MD 20742

Dr. N. C. Luhmann, Jr.
UCLA
7702 Boelter Hall
Los Angeles, CA 90024

Dr. A. Luccio
Brookhaven National Laboratory
Accelerator Dept.
Upton, NY 11973

Prof. J.M.J. Madey
117 Physics Bldg.
Duke University
Durham, NC 27706

Dr. R. Mako
205 South Whiting Street
Alexandria, VA 22304

Dr. Joseph Mangano
Science Research Laboratory
1600 Wilson Blvd.
Suite 1200
Arlington, VA 22209

Dr. Siva A. Mani
Science Applications Intl. Corp.
1040 Waltham Street
Lexington, MA 02173-8027

Dr. T. C. Marshall
Applied Physics Department
Columbia University
New York, NY 10027

Dr. Xavier K. Maruyama
Dept. of Physics
Naval Postgraduate School
Monterey, CA 93943

Dr. B. McVey
Los Alamos National Laboratory
P. O. Box 1663
Los Alamos, NM 87545

Dr. David Merritt
Space & Naval Warfare Command
Attn: PMW 145A
Washington, DC 20363-5100

Dr. A. Mondelli
Science Applications Intl. Corp.
1710 Goodridge Drive
P.O. Box 1303
McLean, VA 22101

Dr. Mel Month
Brookhaven National Laboratories
Associated Universities, Inc.
Upton, L.I., NY 11973

Dr. Gerald T. Moore
University of New Mexico
Albuquerque, NM 87131

Dr. Philip Morton
Stanford Linear Accelerator Center
P.O. Box 4349
Stanford, CA 94305

Prof. J. Nation
224 Phillips Hall
School of Elec. Eng.
Cornell University
Ithaca, NY 14850

Dr. George Neil
TRW
One Space Park
Redondo Beach, CA 90278

Dr. Kelvin Neil
Lawrence Livermore National Lab.
Code L-321, P.O. Box 808
Livermore, CA 94550

Dr. Brian Newnam
MSJ 564
Los Alamos National Scientific Lab.
P.O. Box 1663
Los Alamos, NM 87545

Dr. T. Orzechowski
L-436
Lawrence Livermore National Lab.
P. O. Box 808
Livermore, CA 94550

Prof. E. Ott
Department of Physics
University of Maryland
College Park, MD 20742

OUSDRE (R&AT)
Room 3D1067, The Pentagon
Washington, D.C. 20301

Dr. Robert B. Palmer
Brookhaven National Laboratories
Associated Universities, Inc.
Upton, L.I., NY 11973

Dr. J. Palmer
Hughes Research Laboratory
Malibu, CA 90265

Dr. Richard H. Pantell
Stanford University
Stanford, CA 94305

Dr. Dennis Papadopoulos
Astronomy Department
University of Maryland
College Park, Md. 20742

Dr. John A. Pasour
Mission Research Laboratory
8560 Cinderbed Road
Suite 700
Newington, VA 22122

Dr. C. K. N. Patel
Bell Laboratories
Murray Hill, NJ 07974

Dr. Claudio Pellegrini
Brookhaven National Laboratory
Associated Universities, Inc.
Upton, L.I., NY 11973

Dr. S. Penner
Center for Radiation Research
Natl. Inst. of Standards and Tech.
Gaithersburg, MD 20899

Dr. M. Piestrup
Adelphi Technology
13800 Skyline Blvd. No. 2
Woodside CA 94062

Dr. D. J. Pistoresi
Boeing Aerospace Company
P. O. Box 3999
Seattle, WA 98124-2499

Major E. J. Pogue
SDIO
The Pentagon, T-DE Rm. 1E180
Washington, DC 20301-7100

Major Donald Ponikvar
U. S. Army SDC
P. O. Box 15280
Arlington, VA 22245-0280

Dr. Donald Prosnitz
Lawrence Livermore National Lab.
Box 5511 L-626
Livermore, CA 94550

Dr. D. C. Quimby
Spectra Technology
2755 Northup Way
Bellevue, WA 98004

Dr. G. Ramian
Quantum Institute
University of California
Santa Barbara, CA 93106

Dr. M. Reiser
University of Maryland
Department of Physics
College Park, MD 20742

Dr. S. Ride
Arms Control
Stanford University
Stanford, CA 94305

Dr. C. W. Roberson
Office of Naval Research
Code 112S
800 N. Quincy Street
Arlington, VA 22217

Dr. K. Robinson
Spectra Technology
2755 Northup Way
Bellevue, WA 98004

Dr. Marshall N. Rosenbluth
Dept. of Physics
B-019
Univ. of Calif., San Diego
LaJolla, CA 92093

Dr. N. Rostoker
Department of Physics
University of California at Irvine
Irvine, CA 92717

Dr. A. Saxman
Los Alamos National Scientific Lab.
P. O. Box 1663, MSE523
Los Alamos, NM 87545

Dr. E. T. Scharlemann
L626
Lawrence Livermore National Laboratory
P. O. Box 808
Livermore, CA 94550

Prof. S. P. Schlesinger
Dept. of Electrical Engineering
Columbia University
New York, NY 10027

Dr. Howard Schlossberg
AFOSR
Bolling AFB
Washington, D.C. 20332

Dr. George Schmidt
Stevens Institute of Technology
Physics Department
Hoboken, NJ 07030

Dr. M. J. Schmitt
Los Alamos National Laboratory
P. O. Box 1663
Los Alamos, NM 87545

Dr. H. Schwettmann
Phys. Dept. & High Energy
Physics Laboratory
Stanford University
Stanford, CA 94305

Dr. Marlan O. Scully
Dept. of Physics & Astronomy
Univ. of New Mexico
800 Yale Blvd. NE
Albuquerque, NM 87131

Dr. S. B. Segall
KMS Fusion
3941 Research Park Dr.
P.O. Box 1567
Ann Arbor, MI 4810[illegible]

Prof. P. Serafim
Northeastern University
Boston, MA 02115

Dr. A. M. Sessler
Lawrence Berkeley Laboratory
University of California
1 Cyclotron Road
Berkeley, CA 94720

Dr. W. Sharp
L-626
Lawrence Livermore National Laboratory
P. O. Box 808
Livermore, CA 94550

Dr. Earl D. Shaw
Bell Laboratories
600 Mountain Avenue
Murray Hill, NJ 07974

Dr. R. L. Sheffield
Los Alamos National Laboratory
P.O. Box 1663
Los Alamos, NM 87545

Dr. D. Shoffstall
Boeing Aerospace Company
P.O. Box 3999
Seattle, WA 98124

Dr. Jack Slater
Spectra Technology
2755 Northup Way
Bellevue, WA 98004

Dr. Todd Smith
Hansen Labs
Stanford University
Stanford, CA 94305

Dr. R. Sudan
Lab. of Plasma Studies
Cornell University
Ithaca, NY 14850

Dr. David F. Sutter
ER 224, GTN
Department of Energy
Washington, D.C. 20545

Dr. T. Tajima
Institute for Fusion Studies
University of Texas at Austin
Austin, TX 78712

Dr. R. Temkin
Mass. Institute of Technology
Plasma Fusion Center
Cambridge, MA 02139

Dr. L. Thode
Los Alamos National Laboratory
P. O. Box 1663
Los Alamos, NM 87545

Dr. Norman H. Tolk
Physics Department
Vanderbilt University
Nashville, TN 37240

Dr. Kang Tsang
Science Applications Intl. Corp.
1710 Goodridge Dr.
McLean, VA 22102

Dr. H. S. Uhm
Naval Surface Warfare Center
White Oak Lab.
Silver Spring, MD 20903-5000

Under Secretary of Defense (R&D)
Office of the Secretary of Defense
Room 3E1006, The Pentagon
Washington, D.C. 20301

Dr. John E. Walsh
Wilder Laboratory
Department of Physics (HB 6127)
Dartmouth College
Hanover NH 03755

Dr. Jiunn-Ming Wang
Brookhaven National Laboratories
Associated Universities, Inc.
Upton, L.I., NY 11973

Dr. Roger W. Warren
Los Alamos National Scientific Lab.
P.O. Box 1663
Los Alamos, NM 87545

Dr. J. Watson
Los Alamos National Laboratory
P. O. Box 1663
Los Alamos, NM 87545

Dr. Mark Wilson
Natl. Inst. of Standards and Tech.
Bldg. 245, Rm. B-119
Gaithersburg, MD 20899

Dr. J. Wurtele
M.I.T.
NW 16-234
Plasma Fusion Center
Cambridge, MA 02139

Dr. Ming Xie
Dept. of Physics
Stanford University
Stanford, CA 94305

Dr. Simon S. Yu
Lawrence Livermore National Laboratory
P. O. Box 808
Livermore, CA 94550

Naval Research Laboratory
Washington, DC 20375-5000
Code 4830
Tim Calderwood

Do NOT make labels for
Records-----(01 cy)